SUPPLEMENTARY INFORMATION FOR:

Asymmetric Membrane "Sticky Tape" Enables Simultaneous Relaxation of Area and Curvature in Simulation

Samuel L. Foley and Markus Deserno
Department of Physics, Carnegie Mellon University, Pittsburgh, Pennsylvania
(Dated: January 20, 2024)

I. MODIFIED COOKE LIPID MODEL

The coarse-grained lipid model employed in this work, as illustrated in the main text Fig. 2, is a modified version of the "flip-fixed" model published by the present authors [1], which is itself a modification of the original Cooke lipid model [2, 3]. In this work we made two modifications to the model, the first of which is that each of the four constituent beads of a lipid is scaled according to an angle parameter α which determines the tapered shape of the lipid via

$$\begin{aligned} b_{\mathrm{H}} &= b_0\,(1+3\sin\alpha) - \Delta \\ b_{\mathrm{T1}} &= b_0\,(1+\sin\alpha) \\ b_{\mathrm{T2}} &= b_0\,(1-\sin\alpha) \\ b_{\mathrm{T3}} &= b_0\,(1-3\sin\alpha)\,. \end{aligned} \tag{SI 1}$$

In the above equations, the various b_{X} are the Lennard-Jones self-interaction size parameters for each bead as in

$$U_{\mathrm{LJ}}(r) = 4\varepsilon\left[\left(\frac{b}{r}\right)^{12} - \left(\frac{b}{r}\right)^{6}\right],$$

with H denoting the head bead and T1-3 denoting the 3 tail beads in the model. The original Cooke lipid bead size is $b_0 = 1.0\,\sigma$ (σ being the coarse-grained length unit). Of note is that in the original Cooke model, the head bead is slightly smaller than the tails, having a size of $b_{\mathrm{H}} = 0.95\,\sigma$. Thus the offset $\Delta = 0.05\,\sigma$ above serves to bring our modified bead sizes into agreement with the original model at $\alpha = 0$. The cross-type Lennard-Jones size parameters are all chosen according to the Lorentz mixing rule $b_{ij} = (b_{ii} + b_{jj})/2$. This is the second difference from the previous versions of the Cooke model, as the head-tail interactions originally deviated slightly from the Lorentz rule ($b_{\mathrm{Head-Tail}} = 0.95\,\sigma$ rather than $0.975\,\sigma$). This wrinkle has been removed for simplicity, and was not found to impact the formation of stable fluid lipid bilayers.

This newly redefined model introduces a spectrum of lipids with varying intrinsic curvature preference, but also impacts other properties of the resultant bilayers. In order to characterize this model, various benchmark simulations were carried out in order to measure important membrane properties. The results are summarized in Fig. SI 1 and Table SI 1.

The area per lipid was measured from in-plane-isotropic NPT simulations of flat bilayers with 128 lipids per leaflet (256 total) at zero tension, and dividing the equilibrium average box area (projected membrane area) by 128. The small size of these simulations minimizes the effect of undulations on the measured area. The area modulus $K_{A,\mathrm{m}}$ was found from a linear fit to the surface tension measured from a series of 4 NVT membrane simulations (256 lipids) for each lipid shape, at fixed area strains of 0%, 1%, 2%, and 3%. The bilayer bending modulus κ was measured using the buckling protocol [4, 5], fitting to a stress-strain relation which includes curvature softening [6]. Each κ fit was determined from the results of 4 simulations corresponding to dimensionless buckling strains $\gamma = 10\%$, 20%, 30%, and 40%. For the lipid taper angles α investigated here ($-2°$ through $0.5°$), the number of lipids in the buckle simulations were 1254, 1276, 1292, 1298, 1298, and 1290 respectively. For each α the number of lipids in simulation was the same across all buckling strains γ. The monolayer bending modulus κ_{m} is taken to be $\kappa/2$.

Taper Angle α	$-2°$	$-1.5°$	$-1°$	$-0.5°$	$0°$	$0.5°$
Area per Lipid $[\sigma^2]$	1.276(3)	1.254(4)	1.240(9)	1.233(2)	1.234(3)	1.241(4)
Area Modulus $K_{A,\mathrm{m}}$ $[k_{\mathrm{B}}T/\sigma^2]$	9.6 ± 0.3	10.8 ± 0.3	11.0 ± 0.3	11.8 ± 0.3	12.8 ± 0.3	12.8 ± 0.3
Bending Modulus κ_{m} $[k_{\mathrm{B}}T]$	9.9 ± 1.2	13.2 ± 0.9	13.6 ± 1.0	12.7 ± 1.0	9.7 ± 0.9	6.8 ± 0.8

TABLE SI 1. Relevant material properties of the modified-shape Cooke lipids. Same data plotted in Fig. SI 1

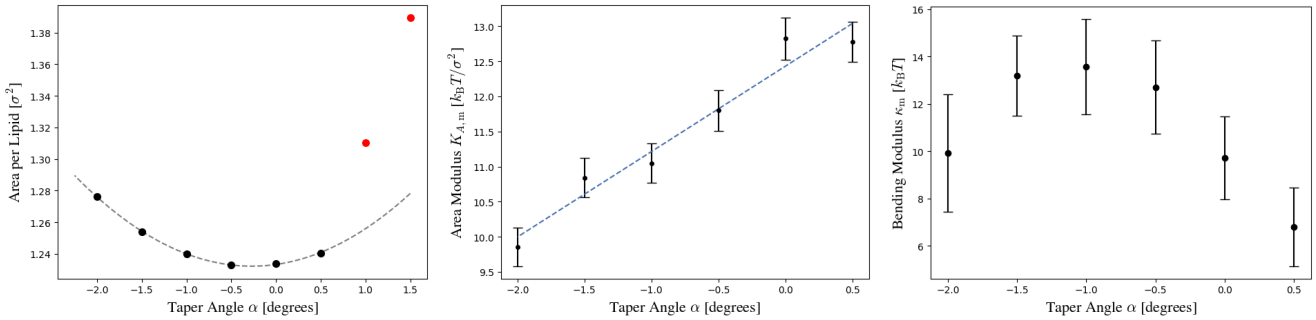

FIG. SI 1. Material properties of lipids in the shape-modified Cooke model employed in this work. From left to right, the plotted data are the area per lipid, monolayer area compressibility modulus $K_{A,\mathrm{m}}$, and monolayer bending modulus κ_m. The data are plotted against the corresponding taper angle that defines the lipid shape according to eqn. SI 1. The two red data points in the area per lipid plot indicate lipid shapes which were not used due to unreliable suppression of flip-flop, and these taper angles are not included in the right two plots. All measurements were made at $k_\mathrm{B}T = 1.5\,\varepsilon$. Errors of the mean in the left plot are smaller than the point markers.

The fluid-gel transition temperature also varies with α. Although we did not quantify this temperature precisely for each lipid shape, we found all those employed here to be in the fluid phase at $k_\mathrm{B}T = 1.5\,\varepsilon$. All the material properties reported here are for symmetric single-component membranes at this temperature.

II. STICKY TAPE IMPLEMENTATION FOR COOKE MEMBRANES

The Cooke lipid-compatible sticky tape consists of two layers of coarse-grained beads arranged in a square lattice, as depicted in Fig. 2 of the main text. In the implementation used throughout this work, each bead is bonded to its nearest neighbors and next-nearest neighbors (see Fig. SI 2) by FENE bonds,

$$U_\mathrm{FENE}(r) = -\frac{1}{2}k_\mathrm{bond}\Delta r_\infty^2 \log\left[1 - \left(\frac{r - r_\mathrm{min}}{\Delta r_\infty}\right)^2\right] , \tag{SI 2}$$

with $k_\mathrm{bond} = 100\,\varepsilon/\sigma$ and $\Delta r_\infty = 0.5\,\varepsilon$. The value of r_min depends on whether the bond in question is between the nearest neighbor or the diagonal next nearest neighbor, as depicted in Fig. SI 2. For nearest-neighbor, $r_\mathrm{min} = r_0 \approx 0.97\,\sigma$, with next-nearest neighbor gaining a factor of $\sqrt{2}$. The exact size of the tape is dependent on the desired simulation geometry, and for all the cases in this work, the box length in the direction of continuous membrane periodicity (into the page in Fig. 2 of the main text) is $L_y = 16\sigma$. With this in mind, each layer of the tape has 16 beads in the direction of membrane periodicity (the length of the tape) and 6 beads in the direction normal to the membrane (the height of the tape), for a total of 96 beads per layer and 192 per tape.

To make the adhesive layer of beads stick to the lipid tails, the tape beads interact with the lipid tail beads via a

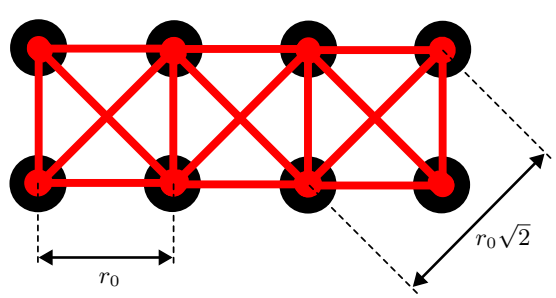

FIG. SI 2. Diagram of the structural bonds which hold together the sticky tape and keep it relatively rigid. Black spheres are sticky tape beads, red lines are FENE bonds (Eqn. SI 2). This bond structure is present both inter- and intra-layer. The indicated lengths give the rest lengths of the corresponding bonded interactions.

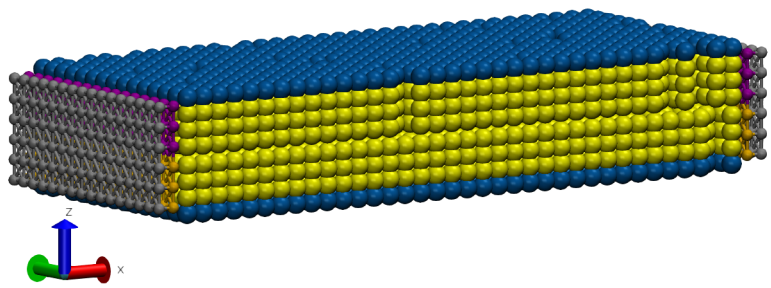

FIG. SI 3. Initial configuration of a Cooke membrane simulation with sticky tape. Blue and yellow beads belong to Cooke lipids; grey, purple, and orange beads comprise the sticky tapes. The membrane is periodic in the y-direction. Snapshot rendered using VMD [8].

Lennard-Jones cosine-squared potential (the same cohesive potential used in the lipid force field, see [3]),

$$U_{\mathrm{LJcos^2}}(r) = \begin{cases} U_{\mathrm{LJ}}(r) & , \quad r < r_{\mathrm{min}} \\ -\varepsilon \cos^2\left[\frac{\pi}{2w}(r - r_{\mathrm{min}})\right] & , \quad r_{\mathrm{min}} \leq r \leq r_{\mathrm{min}} + w \\ 0 & , \quad r > r_{\mathrm{min}} + w \end{cases} . \tag{SI 3}$$

Here $r_{\mathrm{min}} = 2^{1/6} b$ is the minimum of the Lennard-Jones potential and w is the tunable parameter which determines the range of the attractive portion of the potential. For the sticky beads, $w = 1.6\,\sigma$, identical to the lipid tail potentials. The b parameter is determined in the same way as it was above for the tapered lipid beads, using $b_{ii} = 1\,\sigma$ as the effect sticky tape self-interaction size parameter. The top 3 rows of adhesive beads have this attractive potential only for the tail beads of the upper-leaflet lipids, and similarly for the lower beads and lipid tails. For the cross-interactions (upper adhesive beads with lower lipid tails, and vice-versa), a purely repulsive Weeks-Chandler-Anderson potential [7] is employed with b determined in the same manner. The same repulsive potential also acts between the sticky tape and all lipid head beads. The second layer of the sticky tape consists of beads which interact with all lipid beads according to the same kind of repulsive interaction as well.

These precise specifications are simply the ones that we used for all of the simulation. The authors have also successfully implemented sticky tapes using standard harmonic spring potentials rather than FENE bonds, as well as simply bonding every tape bead to every other tape bead within some cutoff distance, rather than the precisely pre-defined scheme of Fig. SI 2. We have provided example simulation files for ESPResSo which implement both of these versions of the sticky tape in conjunction with Cooke lipid membranes, found in `stickytape.py` and `stickytape_autobond.py`.

III. DERIVATION OF EQN. (9)

For the case of identical lipids in both leaflets, combining Eqns. (5) and (6) from the main text gives

$$K_0^\star = \frac{\kappa_{\mathrm{nl}}(A_{0+} - A_{0-})}{z_{\mathrm{n}}(A_{0+} + A_{0-})(\kappa + \kappa_{\mathrm{nl}})}. \tag{SI 4}$$

The monolayer rest areas are assumed to be given by $A_{0\pm} = a_0 N_\pm$, where a_0 is the rest area per lipid. In terms of the asymmetry parameter $\delta n = (N_+ - N_-)/(N_+ + N_-)$ and average number of lipids between the two leaflets $\bar{N} = (N_+ + N_-)/2$, they can also be expressed as $A_{0\pm} = a_0 \bar{N}(1 \pm \delta n)$. Substituting this into the expression given above results in the cancellation of $\bar{N}$, which, along with the definition $\kappa_{\mathrm{nl}} = z_{\mathrm{n}}^2 K_A$, yields Eqn. (9) of the main text.

IV. LATERAL STRETCHING MODULUS PROFILE MEASUREMENT

As laid out by Campelo, et al. [9] the lateral stretching modulus profile can be approximately measured by running several small, flat, PBC simulations at increasing area strain ε_A. By calculating the lateral stress profile $\sigma(z) = \sigma_{||}(z) - \sigma_\perp(z)$ in each simulation, one can numerically approximate $\partial\sigma(z)/\partial\varepsilon_A = \lambda(z)$.

However, there is a rather subtle step in this analysis which is only mentioned as a passing sentence in ref. [9]. Since each successive simulation is at higher area strain, the membrane slightly thins in response. As such, one

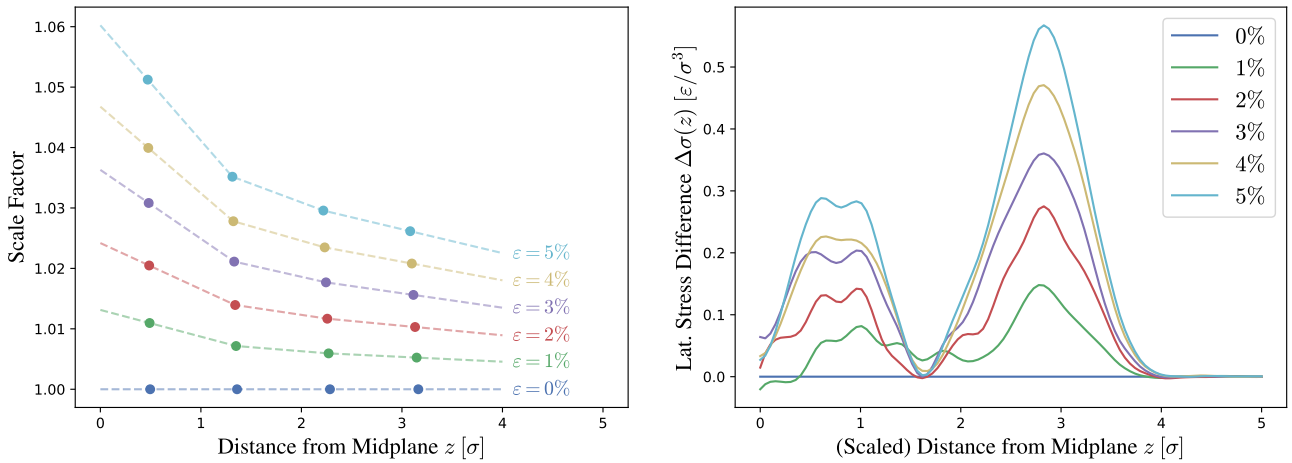

FIG. SI 4. Left: Nonuniform z scaling factors $c_\varepsilon(z)$ for area-strained simulations of an $\alpha = 0.5°$ Cooke lipid membrane. Right: Lateral stress profile differences $\Delta\sigma_\varepsilon(z) = \sigma_\varepsilon(z/c_\varepsilon(z)) - \sigma_0(z)$.

cannot directly compare $\sigma(z)$ profiles from simulations at different area strains; each stress profile from a simulation with $\varepsilon > 0$ must be *scaled* such that the membrane thicknesses match, so that we are comparing $\sigma(z)$ at equivalent *material points* within the membrane. For more finely resolved simulation models with explicit solvent (such as the Martini model used in their study), this is perhaps a straightforward step, as lipid membranes are fairly uniformly incompressible [10], and thus a uniform scaling to match a particular thickness makes sense. This is not so for the Cooke model. As the membrane is stretched, the mean location of each lipid bead varies in a highly non-uniform way, as shown in Fig. SI 4. With this in mind, for each CG bead we calculate $c_\varepsilon = z/z_\varepsilon$, the ratio of the mean position of the given bead in the tensionless configuration to its position in the ε-strained configuration. We then define $c_\varepsilon(z)$ as the linear interpolation of these points, shown as the dotted lines in the first plot of Fig. SI 4. We can then use this scale factor function to calculate the difference between stress profiles measured in simulations at different strains,

$$\Delta\sigma_\varepsilon(z) = \sigma_\varepsilon(z/c_\varepsilon(z)) - \sigma_0(z), \tag{SI 5}$$

as shown in the second plot of Fig. SI 4. Notice that features such as peaks and troughs are roughly aligned in this plot; this is not so without the scaling function. Attempting the analysis using a uniform scaling rather than the more careful scaling done here results in seemingly implausible stretching modulus profiles with significant regions of negative stretching modulus, as well as a very large disagreement between the two measurement methods for z_N.

V. HEXATIC ORDER PARAMETER DISTRIBUTIONS

The magnitude of the hexatic order parameter

$$\psi_6 = \frac{1}{N}\sum_{k=1}^{N} e^{6i\theta_k} \tag{SI 6}$$

is a highly informative order parameter for membrane phase transitions. Here N is the number of nearest neighbors of a given lipid and θ_k is the angle to each nearest neighbor from some fixed axis. $|\psi_6|$ varies between 0 and 1, with 1 corresponding to a perfectly crystalline arrangement. Fig. SI 5 shows examples of $|\psi_6|$ histograms measured in flat PBC simulations below and above the main (fluid-gel) phase transition. Fig. 6 in the main text demonstrates that the ensemble average $\langle|\psi_6|\rangle$ remains unchanged from its equilibrium PBC value in the bulk phase sufficiently far from the membrane edge. This figure only reports data from one flat symmetric membrane simulation, and additionally only shows the mean order parameter rather than the equilibrium distribution.

We wish to demonstrate more thoroughly that the membrane order in the bulk phase is relatively unperturbed by the introduction of adhesive patches and curvature. To this end, for each open-edge adhesive simulation, we carried out a corresponding flat PBC simulation in which the area strain in each leaflet approximately matches that in the open-edge simulation. The details of both the patched-edge simulations and the area-strain-matched simulations are given in Table SI 2. Fig. SI 6 displays the measured $|\psi_6|$ histograms from the bulk phase (discarding data from

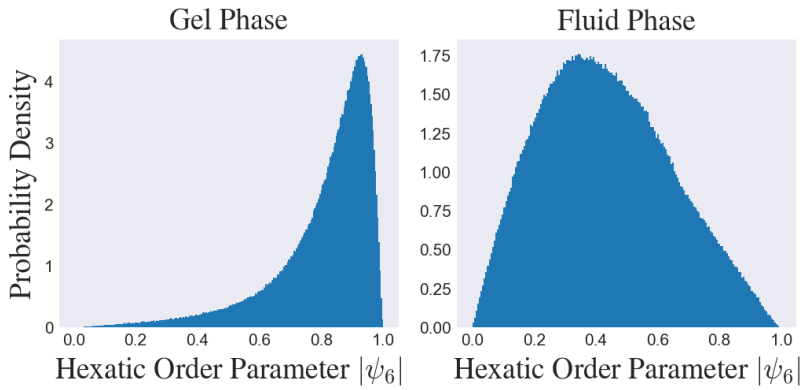

FIG. SI 5. Empirical $|\psi_6|$ order parameter distributions demonstrating the qualitative difference in distribution for fluid and gel states. Both distributions come from a tensionless symmetric $\alpha = 0°$ lipid membrane under periodic boundary conditions. Gel data taken at $k_\mathrm{B}T \approx 1.25\,\varepsilon$, fluid data taken at $k_\mathrm{B}T \approx 1.5\,\varepsilon$.

the membrane edges) in each simulation, with the results from the open-edge (blue data) and corresponding strain-matched (yellow data) systems superimposed on one another. For all corresponding simulations, the mean order parameter is the same within error (not shown), and indeed the distributions themselves are nearly imperceptibly different by eye (the regions which appear green in the plots are overlap of the blue and orange distributions). Rather than delve into precise geometric statistical measures of distance between these distributions, we will simply remark that bulk membrane structure appears to agree between patched-open-edge and fully-PBC simulations to a very high degree. Moreover, comparison of the $|\psi_6|$ distributions in Fig. SI 6 with those shown in Fig. SI 5 confirms that both leaflets remain in the fluid phase for all state points investigated in this work.

[1] S. Foley and M. Deserno, Stabilizing leaflet asymmetry under differential stress in a highly coarse-grained lipid membrane model, Journal of Chemical Theory and Computation **16**, 7195 (2020).
[2] I. R. Cooke and M. Deserno, Solvent-free model for self-assembling fluid bilayer membranes: stabilization of the fluid phase based on broad attractive tail potentials, The Journal of chemical physics **123**, 224710 (2005).
[3] I. R. Cooke, K. Kremer, and M. Deserno, Tunable generic model for fluid bilayer membranes, Physical Review E **72**, 011506 (2005).
[4] H. Noguchi, Anisotropic surface tension of buckled fluid membranes, Physical Review E **83**, 061919 (2011).
[5] M. Hu, P. Diggins IV, and M. Deserno, Determining the bending modulus of a lipid membrane by simulating buckling, The Journal of chemical physics **138**, 214110 (2013).
[6] P. Diggins IV, Z. A. McDargh, and M. Deserno, Curvature softening and negative compressibility of gel-phase lipid membranes, Journal of the American Chemical Society **137**, 12752 (2015).
[7] J. D. Weeks, D. Chandler, and H. C. Andersen, Role of repulsive forces in determining the equilibrium structure of simple liquids, The Journal of chemical physics **54**, 5237 (1971).
[8] W. Humphrey, A. Dalke, and K. Schulten, VMD – Visual Molecular Dynamics, Journal of Molecular Graphics **14**, 33 (1996).
[9] F. Campelo, C. Arnarez, S. J. Marrink, and M. M. Kozlov, Helfrich model of membrane bending: from gibbs theory of liquid interfaces to membranes as thick anisotropic elastic layers, Advances in colloid and interface science **208**, 25 (2014).
[10] M. M. Terzi, M. Deserno, and J. F. Nagle, Mechanical properties of lipid bilayers: A note on the poisson ratio, Soft matter **15**, 9085 (2019).

$\alpha_+ = \alpha_- = 0^\circ$					
N_+	512	522	532	543	553
N_-	512	502	492	481	471
a_+ $[\sigma^2]$	1.2339(3)	1.2249(3)	1.2167(3)	1.2081(3)	1.2017(3)
a_- $[\sigma^2]$	1.2342(3)	1.2437(3)	1.2541(3)	1.2665(3)	1.2777(4)
L^{m} $[\sigma]$	25.136	25.238	25.343	25.469	25.571
N_+^{m}	512	520	528	537	544
N_-^{m}	512	512	512	512	512

$\alpha_+ = -1^\circ, \quad \alpha_- = 0.5^\circ$					
N_+	512	522	532	543	553
N_-	512	502	492	481	471
a_+ $[\sigma^2]$	1.2018(4)	1.1976(3)	1.1937(4)	1.1912(5)	1.1894(4)
a_- $[\sigma^2]$	1.2801(7)	1.2933(8)	1.3067(12)	1.3229(14)	1.3394(21)
L^{m} $[\sigma]$	25.595	25.735	25.858	26.032	26.195
N_+^{m}	545	553	560	569	577
N_-^{m}	512	512	512	512	512

$\alpha_+ = 0^\circ, \quad \alpha_- = -1.5^\circ$					
N_+	512	502	492	481	471
N_-	512	522	532	543	553
a_+ $[\sigma^2]$	1.2817(5)	1.2945(6)	1.3088(7)	1.3243(10)	1.3393(12)
a_- $[\sigma^2]$	1.2080(3)	1.2056(4)	1.2038(3)	1.2030(4)	1.2031(5)
L^{m} $[\sigma]$	25.614	25.749	25.8925	26.045	26.188
N_+^{m}	512	512	512	512	512
N_-^{m}	543	550	557	564	570

TABLE SI 2. Details of the three adhesive-patched membrane strip simulations and the equivalently-area-strained flat NVT PBC simulations. The top part of each table details the simulations with adhesive patches, with the bottom part of each table giving the cubic box dimension L^{m} and number of lipids $N_\pm^{\mathrm{m}}$ in the upper and lower leaflet of the strain-matched simulation.

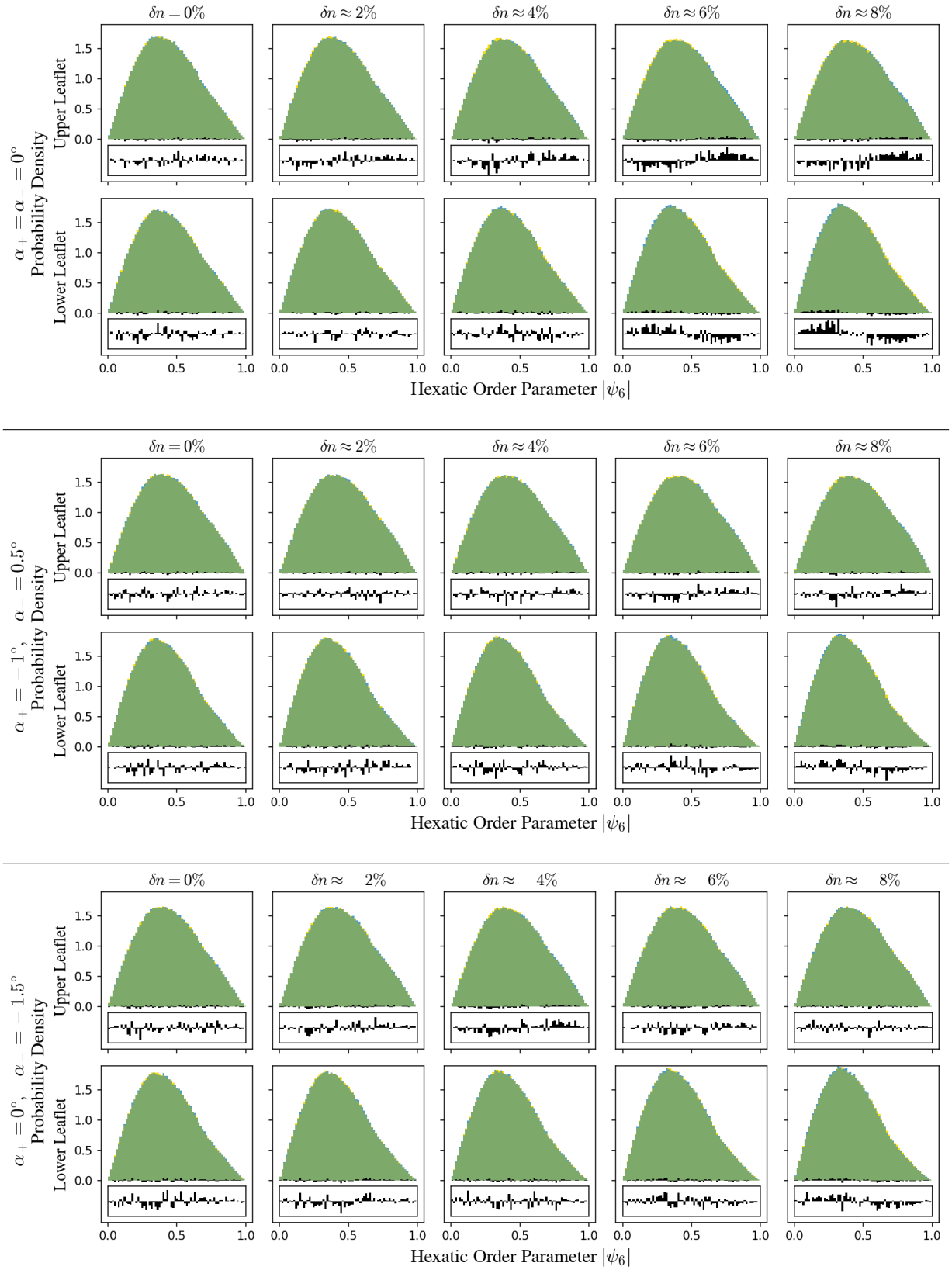

FIG. SI 6. Hexatic order parameter $|\psi_6|$ distributions from adhesive-patched open edge simulations compared against corresponding distributions from flat PBC simulations. The data from the three simulation series are presented in the same order as in Table SI 2. The inset axes show a zoomed-in view of the difference of the histograms, with $y_{\min} = -0.06$ and $y_{\max} = 0.06$ (y-axis scaling of $\sim 4\times$).